Controlling the oxygen species density distributions in the flowing afterglow of O_2/Ar-O_2 surface-wave microwave discharges

Kinga Kutasi[1] §, Rok Zaplotnik[2], Gregor Primc[2], Miran Mozetic[2]

[1]Institute for Solid State Physics and Optics, Wigner Research Centre for Physics, Hungarian Academy of Sciences, POB 49, H-1525 Budapest, Hungary
[2]Jozef Stefan Institute, Jamova cesta 39, SI-1000 Ljubljana, Slovenia

Abstract. The evolution of species densities along a reactor perpendicularly positioned on an O_2 surface-wave microwave discharge is investigated by means of modelling with the aim to define the density tuning possibilities. The validity of the models is shown by the comparison of the calculated and measured axial distribution of O-atoms. The calculations revealed that due to the perpendicular injection of the plasma into reactor the gas temperature is close to the room temperature in most part of it, except a 5 cm region around the inlet. It is shown that the pressure drop along the discharge tube, which results the change of pressure in the discharge region with the gas flow rate induces the variation of the relative density of active species entering the reactor, where the pressure is kept constant. The surface recombination probability of atoms varies along the afterglow tube due to the surface temperature gradient, as well as due to the conditioning of the surface resulting from the continuous operation of the system. The system is shown to be very practical in applications where surfaces/porous materials are to be treated homogeneously by pumping active species through them, since by tuning the gas flow rate equidensity surfaces can be obtained in the case of the two most abundant species, the O-atoms and O_2(a) molecules. In the case of O-atoms the densities obtained at the two pressures investigated, i.e. 100 Pa and 50 Pa, are very similar, as well as their evolution along the reactor, while the density of O_2(a) molecules decreases considerably with pressure.

§ e-mail: kinga.kutasi@wigner.mta.hu

1. Introduction

An efficient method for modification of surfaces of solid materials is treatment with non-equilibrium oxygen content plasma. The technique found broad application in various fields of applied physics from synthesis of nanoparticles to modification of organic materials. Most metals oxidize upon exposure to oxygen plasma. While in some cases rather uniform oxide films are formed, several authors reported formation of oxides with interesting morphology. Since the original report of synthesizing large quantities of single crystalline niobium oxide nanowires in 2005 [1] several authors have reported growth of different nanoparticles on surfaces of a variety of metals [2, 3, 4, 5, 6]. Oxygen plasma treatment is also currently used routinely for hydrophilization of almost all known polymers [7, 8, 9, 10, 11, 12]. The treatment of medical implants in order to improve the biocompatibility upon contact with human blood is widely spread [13, 14, 15, 16], while sterilization of delicate materials using oxygen or oxygen-containing plasma has been elaborated to details [17, 18, 19, 20, 21, 22, 23, 24, 25].

Oxygen discharges can be sustained in a wide pressure range – from mbar to atmospheric pressure – in small diameter dielectric tubes (typically 5-30 mm) by surface propagating electromagnetic waves [26]. By using flowing gas the active species created in the discharge region can be delivered into an afterglow reactor of considerably higher volume than that of the discharge [27, 28]. This system offers a broad range of possibilities in what concerns its applications [29]. The composition of the afterglow plasma required by a given application can be controlled by the discharge conditions, initial gas mixture composition, gas flow rate and the system configuration (e.g. distance from the active plasma to the afterglow chamber) [29]. Surface effects caused by treatment of samples with oxygen plasma depend on the properties of samples including surface temperature and the fluxes of different reactive oxygen particles onto the surface of the samples. In some applications like synthesis of metal oxide nanowires, rather large flux of positively charged oxygen ions is needed in order to accomplish the growth of nanowires in a reasonable time. On the other hand there are delicate organic materials which can be highly damaged when exposed to large fluxes of energetic ions. Consequently, from the application point of view one of the most important plasma characteristics is the density distribution of the plasma species in the afterglow reactor under different discharge conditions, which makes possible to choose the right conditions for the given applications. It has been shown that the density of oxygen species in the flowing afterglow [29, 30] strongly depend on the surface reactions, i.e. heterogeneous surface recombination, whose probability depends enormously on the type of material facing plasma or afterglow, as well as the surface finish of these materials. Values of recombination coefficient vary for several orders of magnitude from some glasses with recombination coefficient below 10^{-4} [31] to some metals with coefficients well over 0.1 [30, 32]. In our present work we concentrate on the effect of the system configuration, i.e. the tuning possibilities of the species densities offered by the gas flow rate and a specific system geometry.

Experimentally it is easily accessible the density of oxygen atoms, which can be determined in the afterglow by using a catalytic probe, especially the fiber-optics version [33, 34]. This technique makes also possible the determination of the axial distribution of the densities along a reactor. A semi-quantitative method often applied for characterization of plasma created in a mixture of argon and oxygen is actinometry [35, 36], while a variety of optical absorption techniques are used for determination of the O-atom density also in oxygen plasma afterglow [37, 38]. However, the absolute density of the metastable state oxygen molecules, that also play important role in applications [39], is more difficult to determine. The density of active species downstream of a surface-wave microwave discharge has been recently measured with the help of mass spectrometry [40], which is a promising tool for the future characterization of these flowing afterglows, making accessible also the density $O_2(a)$ molecules, although not their distribution along the reactor. For the determination of all the species density distributions in the whole reactor volume the plasma modelling appears as a unique possibility. When complemented with experimental measurements the validated discharge and afterglow models can reveal the evolution of the species along the whole system, as well as the temperature distribution and the flow dynamics.

In the present work the density distributions of the active species in an afterglow reactor perpendicularly positioned on a flowing surface-wave microwave discharge are determined by means of discharge kinetic and 3-D afterglow hydrodynamic models, that have been validated through comparison of the measured and calculated axial distribution of oxygen atom densities. The experimental system and methods are presented in Section 2, while the models applied are described in Section 3. The expansion of the plasma in the afterglow reactor and the evolution of the species density in the reactor under different gas mixture, pressure and flow conditions are discussed in Section 4.

2. Experimental arrangement, methods and operating conditions

The system used in the present study is presented schematically in Figure 1. The system is built from high-vacuum compatible materials using Viton gaskets. Commercially available oxygen of purity 99.99% and Ar of same purity are leaked into the system through mass flow controllers Aera FC-770CD. The discharge is ignited in a Quartz tube of inner and outer diameters 6 and 8 mm, respectively, using a water cooled surfatron type 80, connected to 2.45 GHz Sairem GMP 03 KED B microwave generator. The discharge tube is mounted perpendicularly to the afterglow chamber, which is closed with a blank flange on one end and connected to a vacuum pump on the other end. There is an adjustable orifice (MKS Type 253B Exhaust Throttle Valve) between the afterglow chamber and the pump so that the effective pumping speed is adjustable. We used a two-stage mechanical rotary pump with the nominal pumping speed of 80 m^3/h and the ultimate pressure below 0.1 Pa. Pressure is measured on the closed end of the afterglow chamber and at the inlet of the discharge tube with calibrated absolute

vacuum gauges MKS Baratron 722A. The system is open frequently and never baked so the residual atmosphere contains practically only water vapor.

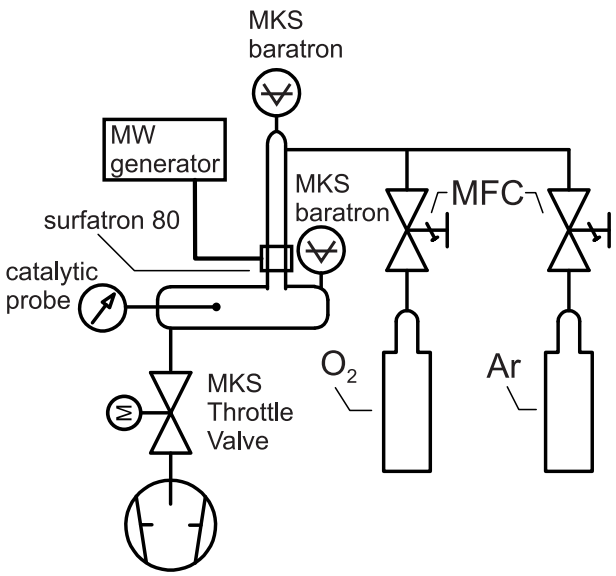

Figure 1. Schematic view of the system set-up.

A detailed drawing of the discharge and afterglow tubes is presented in Figure 2. The 51 cm Quartz tube is mounted perpendicularly to the afterglow chamber, that is 74 cm long Pyrex tube with 36 mm inner diameter, and it enters a few cm's . The Pyrex tube on one end terminates with a standard KF40 tee made from stainless steel, where the vacuum gauge is mounted onto. The other end of the Pyrex tube is connected to the vacuum pump through a series of tees. Here a simple air inlet valve is mounted for venting the whole vacuum system, as well as a movable catalytic probe as shown in Figure 2. The probe could be moved all the way along the Pyrex tube in order to allow for longitudinally resolved measurements of the density of neutral oxygen atoms in the ground state. We used a standard thermocouple catalytic probe with cobalt as the sensing material. The voltage of the thermocouple is sampled automatically in 0.1 s intervals and the volt-meter is connected to a computer for data acquisition and processing.

Sensing of neutral oxygen atoms by catalytic probes have been explained to details elsewhere [34]. Due to completeness of this paper let us just mention the basic principle. Pure cobalt exhibits catalytic recombination of the O-atoms on the surface with a large recombination probability of 0.12 [32]. Extensive surface recombination causes heating of the catalyst. The temperature is monitored in terms of the thermocouple voltage and the O-atoms density is calculated from the thermocouple signal using appropriate physical formalism. The addition of argon does not influence the heterogeneous surface recombination of neutral oxygen atoms and does not disturb the probe signal as long as argon atoms are found in the ground state (that is the case for our conditions [29]). Otherwise, relaxation of argon metastables would cause over-estimation of the neutral

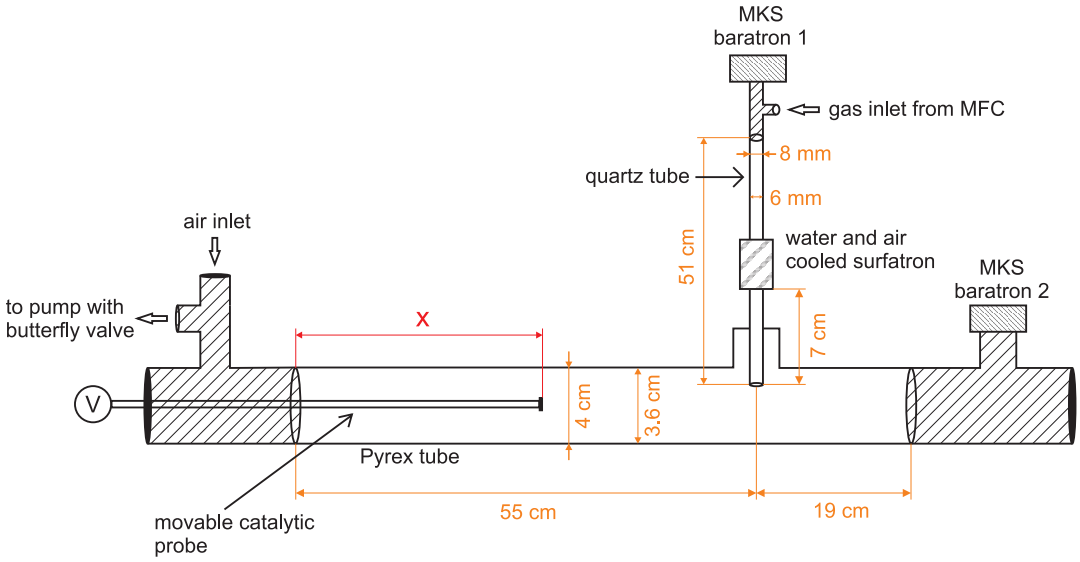

Figure 2. Detailed drawing of the discharge and afterglow tubes.

oxygen atom density in the vicinity of the catalyst.

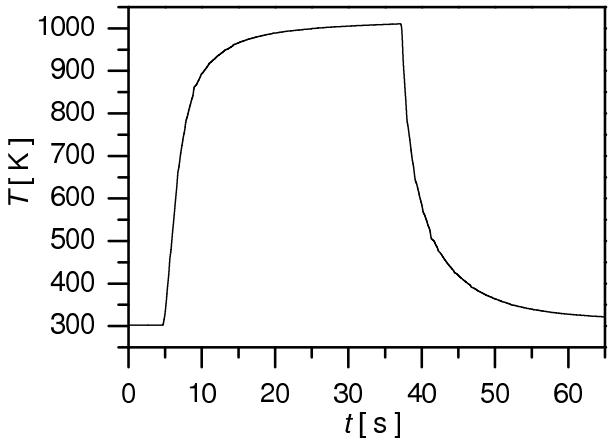

Figure 3. A typical catalytic probe characteristic measured in the afterglow of a pure O_2 discharge at 100 Pa and 290 sccm gas flow rate.

Using the movable catalytic probe the O-atoms density has been measured at 21 different probe positions along the afterglow chamber at two different pressures in the afterglow chamber (50 and 100 Pa), for several different flow rates (50, 75, 100, 115, 135, 125, 210, 290, 340 and 405 sccm) and different gas mixtures with the power on the generator fixed at 150 W. A typical probe characteristic is shown in Figure 3. The characteristics shows the start of the temperature rise with the ignition of the discharge (at 5 s on Figure 3) and its fast increase due to extensive surface recombination of neutral oxygen atoms. The discharge is turned off when the temperature of probe stabilizes, that is here at about 800 K. Such curves were measured at all experimental conditions in order to calculate the density of oxygen atoms in the vicinity of the probe tip [34].

For a better understanding of the measured density features and to reveal the density distribution of all the oxygen species in the whole reactor the modelling investigation of the system has been also conducted at the experimentally studied conditions with the models presented in the next section.

3. Model and important parameters used in modelling

Along the afterglow system three different parts are to be distinguished: (*i*) the discharge region; (*ii*) the early-afterglow region, which develops downstream from the discharge in the small diameter tube; and (iii) the late-afterglow present in the large diameter tube used as treatment reactor. The species generated in the discharge are carried by the gas flow through the early-afterglow region into the post-discharge reactor. The evolution of the species densities in the different parts of the system can be followed with three different models.

The creation of the different species in the discharge is described with a zero dimensional self-consistent kinetic model [41, 42, 43] that is based on the solutions of the electron Boltzmann equation for the microwave field, coupled to a system of rate-balance equations for the neutral and charged heavy species. A detailed description of the model for the case of an Ar-O_2 surface-wave microwave discharge is given in Ref. [47], where the gas phase and surface reactions governing the chemical kinetics of the species Ar($^1S_0$, $^3P_2$, $^3P_1$, $^3P_0$, $^1P_1$), $O_2(X\ ^3\Sigma_g^-$,v), $O_2(a\ ^1\Delta_g$, $b\ ^1\Sigma_g^+$), O(^{3}P, ^{1}D), O_3, Ar^+, $Ar_2{}^+$, $O_2{}^+$, O^+ and O^- are also listed. Since we are interested only in the flowing afterglow, the calculations need to be conducted only for the value of the critical electron density corresponding to the end of the plasma column, which determines the density of species leaving the discharge zone [26, 44]. For surface-wave discharges generated at 2.45 GHz in a quartz tube this electron density is 3.74×10^{11} cm^{-3} [44].

The evolution of the species along the early-afterglow downstream from the discharge is followed with a system of time-dependent rate-balance equations for the different species. Here, the same chemical-kinetics scheme is used as in the discharge region. However, due to the very low electron energies, the electron impact excitation/ionization processes are omitted [29, 45]

The density distribution of species in the reactor entering from the early-afterglow region are calculated with a three dimensional hydrodynamic model as described in Ref. [29, 46]. The hydrodynamic model is composed of (i) the total mass conservation, (ii) the continuity equations for the different species, (iii) the total momentum conservation equation, and (iv) the total energy conservation equation, thus making possible the determination of the velocity field, temperature and density distributions in the reactor. The treatment of the surface recombination processes, that are one of the major losses of active atoms is discussed in details in Ref. [30].

The models besides the reaction rates, that can be found in the literature as described in [47] need several input parameters, which have been determined experimentally. One important parameter is the total gas pressure, which has been

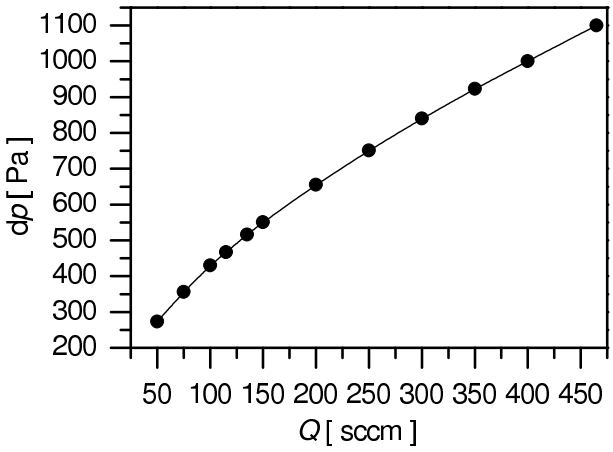

Figure 4. Pressure drop along the 6 mm diameter 51 cm long discharge tube as a function of gas flow rate.

Table 1. Characteristic parameters of different regions in case of O_2 discharge when 100 Pa pressure is kept in the reactor. $L_{\rm dis}$ and $L_{\rm aft}$ denote the length of the discharge and afterglow region, respectively, $t_{\rm aft}$ is the flight-time of species in the afterglow region, while $w_{\rm in}$ is the absolute value of the gas inlet velocity at the reactor entrance. As the pressure along the afterglow region varies, here a medium pressure $p_{\rm m}$ is defined.

Gas flow	Discharge	Early-afterglow	Late-afterglow
405 sccm	$p = 230$ Pa	$p_{\rm m} = 160$ Pa	$w_{\rm in} = 393$ ms^{-1}
	$L_{\rm dis} = 0.5$ cm	$L_{\rm aft} = 6.5$ cm	
		$t_{\rm aft} = 2.2\times10^{-4}$ s	
340 sccm	$p = 220$ Pa	$p_{\rm m} = 160$ Pa	$w_{\rm in} = 330$ ms^{-1}
	$L_{\rm dis} = 0.5$ cm	$L_{\rm aft} = 6.5$ cm	
		$t_{\rm aft} = 2.2\times10^{-4}$ s	
290 sccm	$p = 190$ Pa	$p_{\rm m} = 150$ Pa	$w_{\rm in} = 281$ ms^{-1}
	$L_{\rm dis} = 1$ cm	$L_{\rm aft} = 6$ cm	
		$t_{\rm aft} = 2\times10^{-4}$ s	
210 sccm	$p = 170$ Pa	$p_{\rm m} = 130$ Pa	$w_{\rm in} = 203$ ms^{-1}
	$L_{\rm dis} = 2$ cm	$L_{\rm aft} = 5$ cm	
		$t_{\rm aft} = 2.2\times10^{-4}$ s	
125 sccm	$p = 140$ Pa	$p_{\rm m} = 120$ Pa	$w_{\rm in} = 121$ ms^{-1}
	$L_{\rm dis} =3$ cm	$L_{\rm aft} = 4$ cm	
		$t_{\rm aft} = 2.9\times10^{-4}$ s	

kept constant at 100 Pa and 50 Pa, respectively in the reactor. However, due to the high gas flows - in the range of 50-405 sccm - a large pressure gradient develops along the 6 mm diameter 51 cm long discharge tube. In order to determine the gas pressure values in the different regions of the system - discharge and early-afterglow - the pressure drop along the 6 mm tube, i.e. the pressure difference between the gas inlet and the reactor has been measured. Figure 4 shows the pressure difference as a function of gas flow rate. In a good approximation the pressure at a given gas flow rate drops linearly along the tube. Accordingly, from the measured pressure differences the pressure values

Table 2. Characteristic parameters of different regions in case of O_2 discharge when 50 Pa pressure is kept in the reactor. The parameters are those described at Table 1.

Gas flow	Discharge	Early-afterglow	Late-afterglow
135 sccm	$p = 70$ Pa	$p_m = 60$ Pa	$w_{in} = 263$ ms^{-1}
	$L_{dis} = 5$ cm	$L_{aft} = 2$ cm	
		$t_{aft} = 7\times10^{-5}$ s	
100 sccm	$p = 65$ Pa	$p_m = 60$ Pa	$w_{in} = 195$ ms^{-1}
	$L_{dis} = 5$ cm	$L_{aft} = 2$ cm	
		$t_{aft} = 9\times10^{-5}$ s	
75 sccm	$p = 65$ Pa	$p_m = 57$ Pa	$w_{in} = 146$ ms^{-1}
	$L_{dis} = 5$ cm	$L_{aft} = 2$ cm	
		$t_{aft} = 1.2\times10^{-4}$ s	
50 sccm	$p = 0.6$ mbar	$p_m = 0.56$ mbar	$w_{in} = 97$ ms^{-1}
	$L_{dis} = 5$ cm	$L_{aft} = 2$ cm	
		$t_{aft} = 1.8\times10^{-4}$ s	

at the discharge and early-afterglow regions can be determined by knowing the position of the surfatron and the length of the discharge (also determined experimentally at each condition as listed in Table 1 and Table 2). Furthermore, the flight-time of species, which will determine the relative density of species entering the reactor is calculated from the length of this region and the applied gas flow rate. The data obtained in this way are presented in Table 1 and Table 2 for the two different pressure conditions in the reactor. The gas temperature in the discharge and early afterglow region is taken 500 K, while the temperature of the gas at the reactor inlet is 450 K. The surface recombination probability of the oxygen species in these regions is taken $\gamma_O = 8\times10^{-3}$ in accordance with the results of Macko *et al* [36]. Furthermore, the wall deactivation probabilities of $O(^1D)$, $O_2(a)$ and $O_2(b)$ were taken to be 1, 2×10^{-5} and 2×10^{-2}, respectively [48, 49].

4. Results and Discussion

4.1. Expansion of the plasma in the reactor

As already mentioned the model makes possible the visualization of the gas flow in the reactor. Figure 5 shows the distribution of the two velocity components, i.e. w (z component) and u (x component), in the vertical symmetry plane of the reactor that includes the inlet at $x = 54$ cm. The plasma jet entering the reactor hits the opposite (bottom) wall, creating small turbulence at high gas flow rates, before it starts flowing in the direction of the pumping outlet. As shown by the u profile, opposite to the pumping outlet the plasma species move just by diffusion, the convective velocity being vanishingly small.

The gas temperature in the reactor is strongly influenced by the gas flow rate. Figure 6 shows the temperature profile in the reactor for the highest and lowest gas flow rate used at 100 Pa. At high flow rate the plasma jet cools down slowly reaching

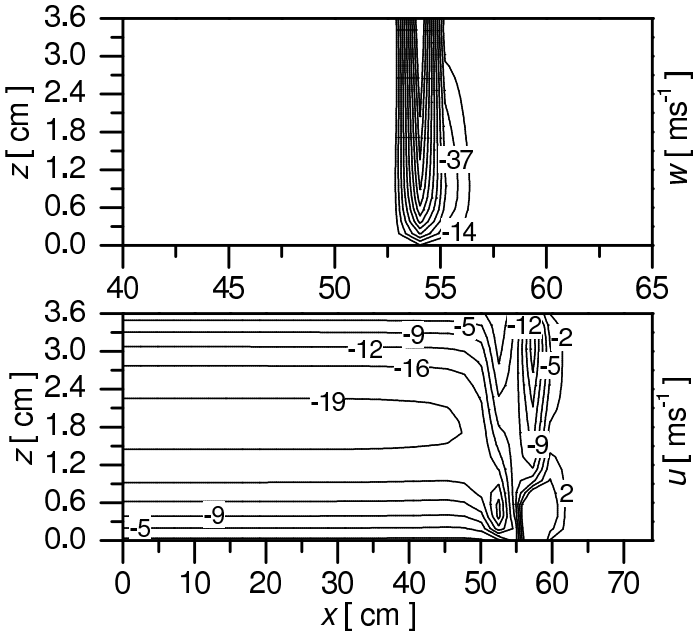

Figure 5. Velocity distributions in the vertical symmetry plane of the reactor at 405 sccm gas flow rate when constant 100 Pa pressure is kept in the reactor. The inlet velocity w_{in} = -393 ms^{-1}.

the bottom wall with still a high gas temperature at around 380 K. However, radially a fast cooling occurs due to the radial expansion of the jet, i.e. within 5 cm the gas temperature reaches 312 K. At low flow rate, due to the lower inlet plasma velocity the gas temperature decreases faster, thus the plasma temperature at the bottom wall is only around 310 K. Similarly, the radial cooling is also faster, 312 K is achieved within 3 cm. Accordingly, at every gas flow condition the gas temperature is around the ambient temperature in most part of the reactor. This is one of the advantages of this configuration, comparing to the systems where the gas inlet is in axis with the pumping outlet. In such a configuration 25 cm is needed to reach a gas temperature of about 312 K.

At the lower pressure here investigated, 50 Pa, with the highest gas flow rate used similar behaviour can be observed (not presented on a figure here) for the plasma expansion as for the lowest gas flow rate used at 100 Pa. Accordingly, at this pressure the plasma cools down before reaching the opposite wall even at the highest gas flow rate used.

4.2. Oxygen species density distributions in the reactor

4.2.1. O_2 discharge As described in Section 2 the density of O-atoms has been measured by means of a catalytic probe along the axis of the reactor, while the hydrodynamic model (Section 3) revealed the density distribution of O-atoms in the whole reactor. The axial distribution of the measured and calculated O-atoms

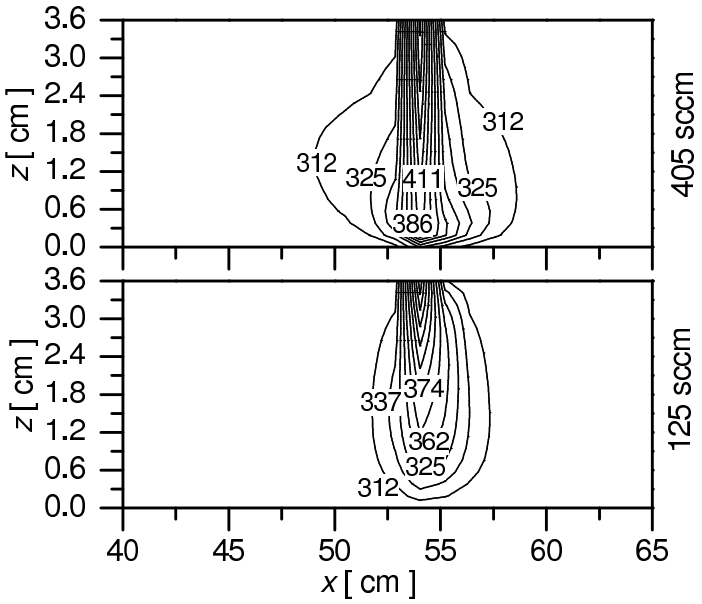

Figure 6. Temperature distributions in the vertical symmetry plane of the reactor at 405 sccm and 125 sccm gas flow rates when constant 100 Pa pressure is kept in the reactor. The inlet temperature is 450 K.

densities are presented in Figure 7. As expected - based on the velocity profiles - the densitydecreases fast in the region dominated by the diffusion, i.e. at distances higher than 55 cm, independently of the gas flow, while towards the outlet the oxygen atoms density decreases moderately depending on the gas flow rate. The experimentally observed features of the density distributions – reproduced by the calculations – can be better understood with the help of modelling. As already suggested by the measured data and brought to light by the higher resolution calculated data shown in Figure 7(b), the density of atoms in the reactor is not the maximum at the inlet axis.

This can occur as a result of the high temperature gradient around the inlet, see Figure 6, due to which a local change of the total gas density develops, namely a minimum density at the maximum temperature position. Therefore, the absolute density of O-atoms can show an increase in the vicinity of the inlet in the flow direction from $x = 55$ cm to 50 cm, where the temperature starts to stabilize (Figure 6).

The evolution of the atoms density in the reactor besides the gas flow is strongly influenced by the surface reactions, i.e. surface recombination of atoms along the reactor wall. The calculations have shown, that due to the fact that the measurements have been conducted under continuous operation of the discharge the conditioning of the reactor's surface occurred. As a consequence, the decrease of the O-atoms recombination on the wall has been observed during the measurements. The experimentally measured density profiles could be reproduced by choosing $\gamma_O = 10^{-3}$ at the 405 sccm flow condition, $8{\times}10^{-4}$ at 340 sccm and 290 sccm, $6{\times}10^{-4}$ at 210 sccm and $5{\times}10^{-4}$ at 125 sccm. However, the comparison of the measured and calculated profiles has shown that the calculated profiles are broader than the measured ones, suggesting that the surface

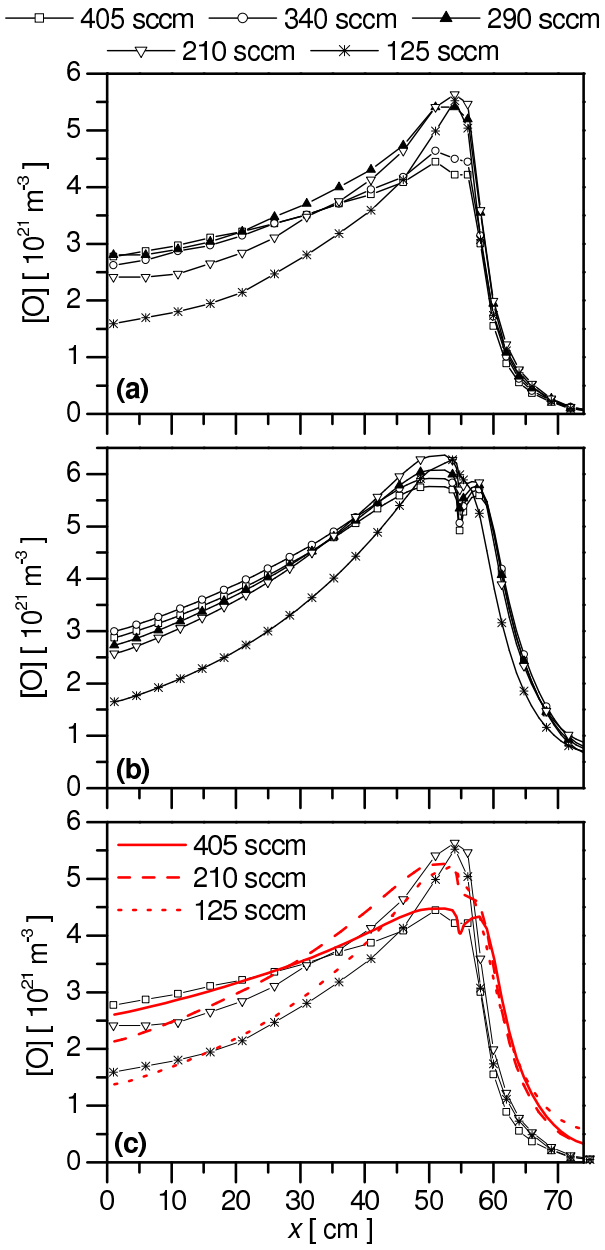

Figure 7. Measured (a) and calculated (b) oxygen atom densities along the middle axis of the reactor at different gas flow rates when the pressure in the reactor is kept constant at 100 Pa. (c) Comparison of measured densities with normalized calculated densities. At the highest flow the variation of the surface recombination probability of atoms along the reactor, as shown in Figure 8, is taken into account.

recombination of the atoms is not constant along the tube. This inhomogeneity can be explained first of all by the gradient of the wall temperature, which influences the recombination of atoms on the surface. As shown in Figure 8(a) at the wall opposite to the inlet considerably higher temperatures can occur than in the other parts of the reactor. At the bottom wall, as also shown by Figure 6, the temperature diminishes with decreasing the gas flow rate. The densities have been recalculated by choosing

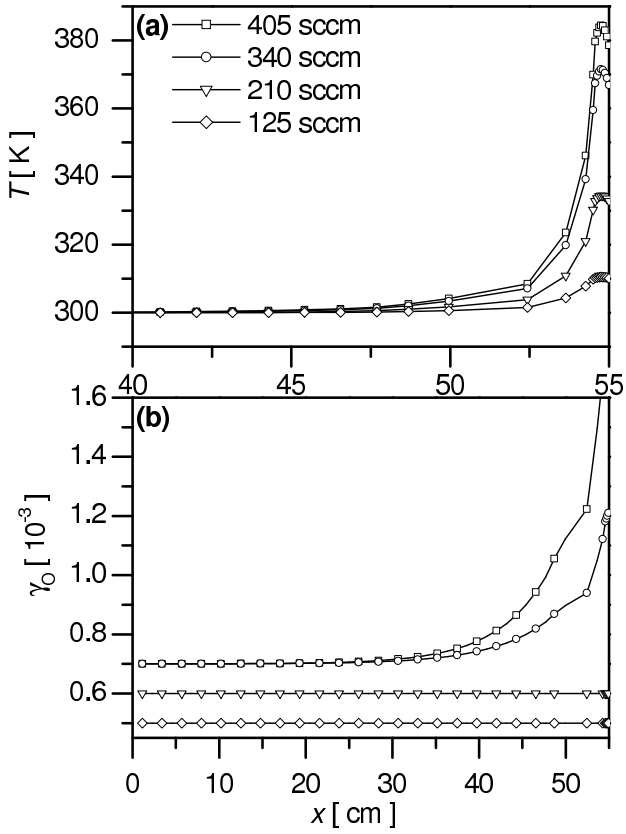

Figure 8. (a) Axial distribution of the temperature at the bottom of the reactor and (b) the assumed variation of the surface recombination probability of the oxygen atoms along the reactor.

surface recombination probabilities in accordance with the temperature profile at the surface as shown in Figure 8(b). Figure 7(c) shows the densities calculated with these newly set γ_O values and the measured densities for selected gas flow rate conditions at 100 Pa. The calculated densities have been normalized to the measured densities, using a normalization factor of 1.2. The catalytic probe used for density measurements is a drain for neutral oxygen atoms and therefore lowers the O-atoms density in its vicinity. Due to the probes influence on the local density, the measured density is lower than the density on the probe position without its presence.

Although the temperature dependent surface recombination probability of atoms resulted in distributions that are in a good agreement with the measured ones, some discrepancies can still be observed, suggesting that the surface recombination along the reactor is not only influenced by the temperature, but also by the conditioning of the surface. The surface conditioning depends on the flux of active species reaching it, which varies along the flow. On the diffusion governed region, where the active species flux is very low the surface is less conditioned, therefore the surface recombination probability is higher. This can be concluded from the fact that the normalized calculated densities here are higher than the measured ones. The variation of the surface recombination

probability along the reactor due to the temperature gradient and the conditioning of the surface is a very important effect, that should be taken into account when systems are designed for applications, and especially when long run treatments of bulky samples are planned.

As already mentioned the modelling calculations reveal the density distribution of all the species in the reactor, thus making possible to gain information also about the species that are difficult to trace by experimental methods. Figure 9 and Figure 10 show the distribution of oxygen atoms and O_2(a) molecules – being the most important [39, 50] and abundant oxygen species [29] – in the vertical symmetry plane of the reactor at different gas flow rates, when 100 Pa pressure is kept in the reactor. The two species density distributions show very similar features, as both densities are mostly controlled at this pressure by the surface processes. On the density distributions, i.e. on the shape of the equidensity surfaces the effect of the gas flow can be easily identified. These surfaces tend towards planes with decreasing flow. Nonetheless, the O_2(a) molecules density at the highest flow in the flow dominated region changes only slightly.

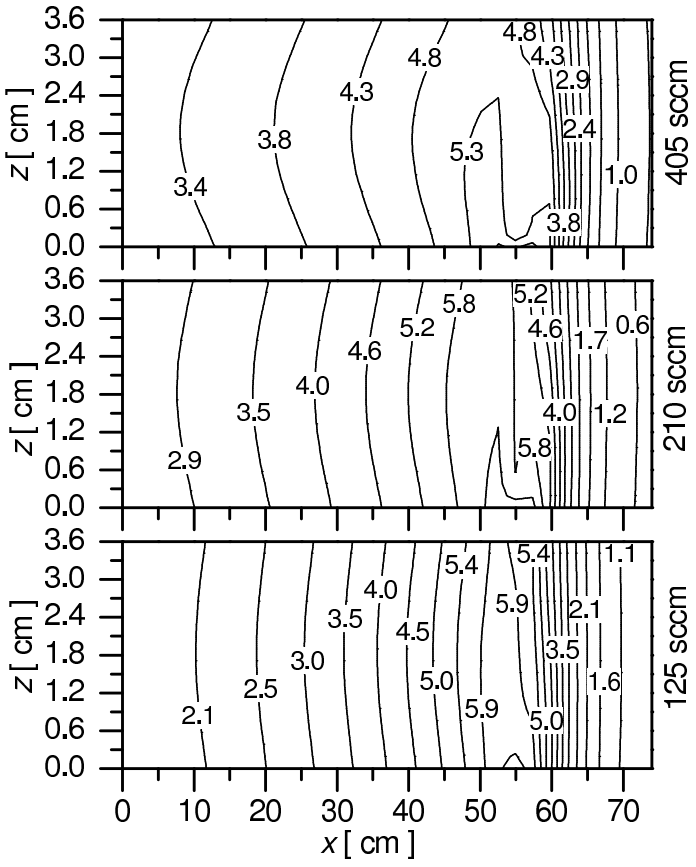

Figure 9. Calculated oxygen atom density distributions in the vertical symmetry plane of the reactor at different gas flow rates at 100 Pa. The densities are given in 10^{21} m^{-3} units.

The density distributions of further oxygen species – namely O_2(b) and O_3 – are shown in Figure 11. The densities of these molecules vary considerably along the reactor

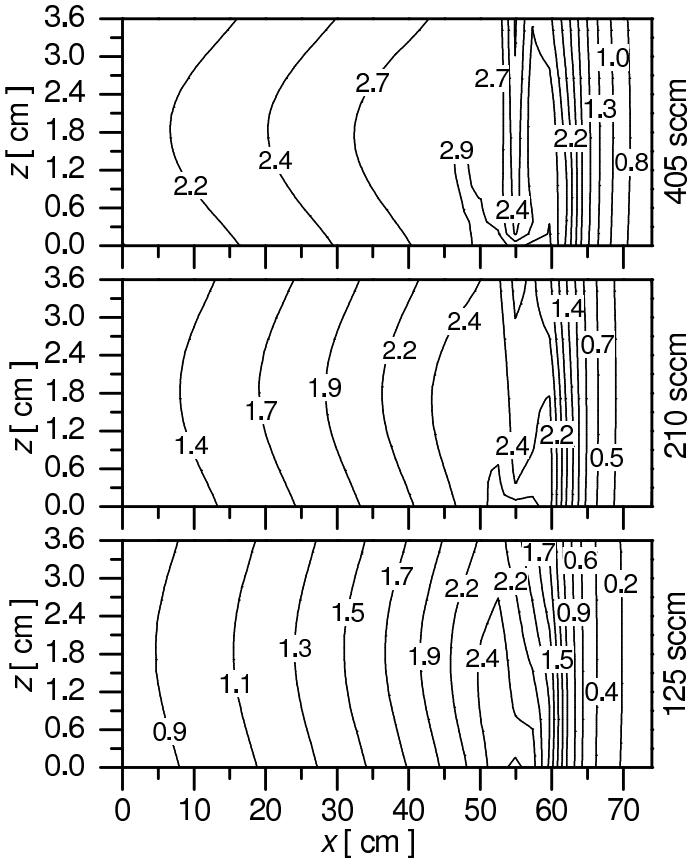

Figure 10. Calculated O_2(a) density distributions in the vertical symmetry plane of the reactor at different gas flow rates at 100 Pa. The densities are given in 10^{21} m^{-3} units.

as shown by their axial distributions. In the afterglow the recombination of O_2(b) molecules is very fast, which occurs mostly due to the quenching by O-atoms. On the contrary, the ozone density increases as a result of the disappearance of its more efficient quenchers the O_2(b) molecules and O(^{1}D) excited atoms.

With reducing the gas pressure the loss of active species through the three body recombination processes can be decreased. Therefore the density distribution of species has been studied at a lower pressure, namely 50 Pa, which was kept constant in the reactor. However due to the pumping limit of the vacuum pump the lower pressure in the reactor could be achieved only by applying lower gas flow rates, which can result in a faster density decay along the reactor. Figure 12 shows the axial distribution of measured and calculated O-atoms density at different gas flow rates. Comparing to the 100 Pa case at 50 Pa the absolute densities at the inlet are lower, however in a large part of the reactor densities close to that of 100 Pa case can be achieved. Figure 12(a) shows the comparison between the calculated and measured density distributions. The discrepancies between the densities here observed, can originate from the surface recombination of atoms, since in calculations the surface recombination probability is taken constant along the tube. The variation of the surface recombination probability due to the surface temperature

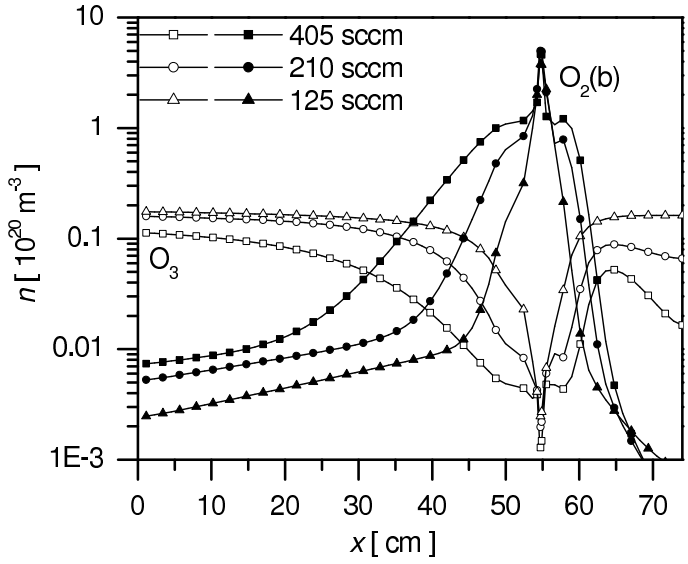

Figure 11. Calculated densities of O_2(b) and O_3 molecules along the reactor at different gas flow rates when the pressure in the reactor is kept constant at 100 Pa.

gradient is not justified at these conditions, however due to the continuous run of the system the surface conditioning occurs. As along the reactor the tube surface is subjected to a varying species flux the surface conditioning along the tube is not constant.

As already shown at the 100 Pa case the density distributions of O-atoms and O_2(a) molecules in the reactor are very similar. Here we show the calculated density distribution of O_2(a) molecules in the vertical symmetry plane of the reactor. The distributions are very similar to those obtained at 100 Pa, however at this pressure the molecular densities are considerably lower. Guerra *et al* [51] have shown that the relative density of O_2(a) molecules increases with pressure, a sharp increase being observed in the 50-400 Pa pressure range [29]. As a consequence, with decreasing the pressure the effect of O_2(a) molecules in application processes can be eliminated, as well as using the pressure as a control parameter the effect of these species in different processes can be studied. Concerning the densities of the other oxygen species, the O_2(b) and ozone, similar behaviour (not shown here) can be observed as at 100 Pa, with absolute densities orders of magnitude lower in most part of the reactor than that of the O-atoms (i.e. the maximum density of O_2(b) at the inlet is in the 10^{20} – 3×10^{20} m^{-3} range and decreases to 10^{18} m^{-3}, while the O_3 density increases from 10^{18} m^{-3} at inlet to 3×10^{19} m^{-3} at outlet).

4.2.2. Ar-O_2 discharge The addition of noble gases to molecular gas discharges can decrease the efficiency of the gas heating. The increase of Ar content of the mixture may result in the decrease of the absolute density of oxygen species, nevertheless the introduced noble gases contribute to a more efficient dissociation of the O_2 molecules.

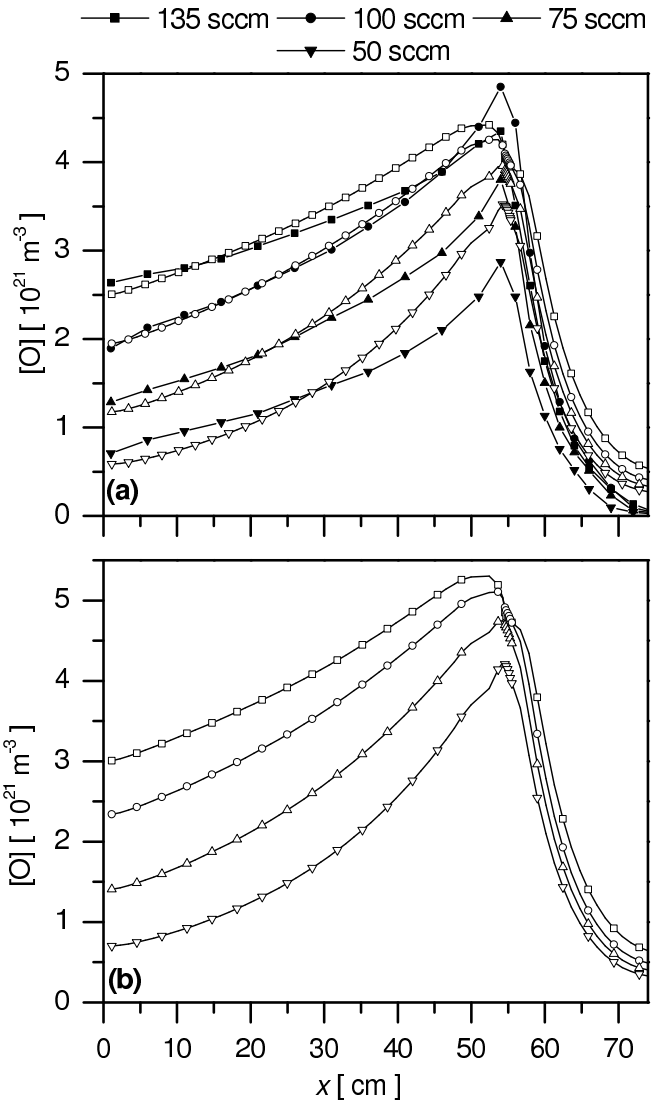

Figure 12. (a) Comparison of measured (full symbols) and normalized calculated (open symbols) oxygen atom densities, and (b) calculated oxygen atom densities along the middle axis of the reactor at different gas flow rates, when the pressure in the reactor is kept constant at 50 Pa.

The dissociation of O_2 molecules has been found to increase with Ar addition and to depend on the gas pressure in the discharge region, i.e. it has a minimum at around 400 Pa depending on the mixture composition when the discharge exciting frequency is 2.45 GHz [52]. In this way the density of O-atoms can be kept at reasonable level at a lower gas temperature, while the ratio of atomic to molecular oxygen species densities can also be tuned. The effect of Ar on the density distributions in the reactor has been studied in a 90%O_2-10%Ar mixture at 100 Pa.

Figure 14 shows the axial distribution of O-atoms at different gas flow rates. Comparing to the 100% O_2 case at the inlet slightly lower O densities can be achieved. The biggest difference occurs at the lowest gas flow rate used due to the fact, that

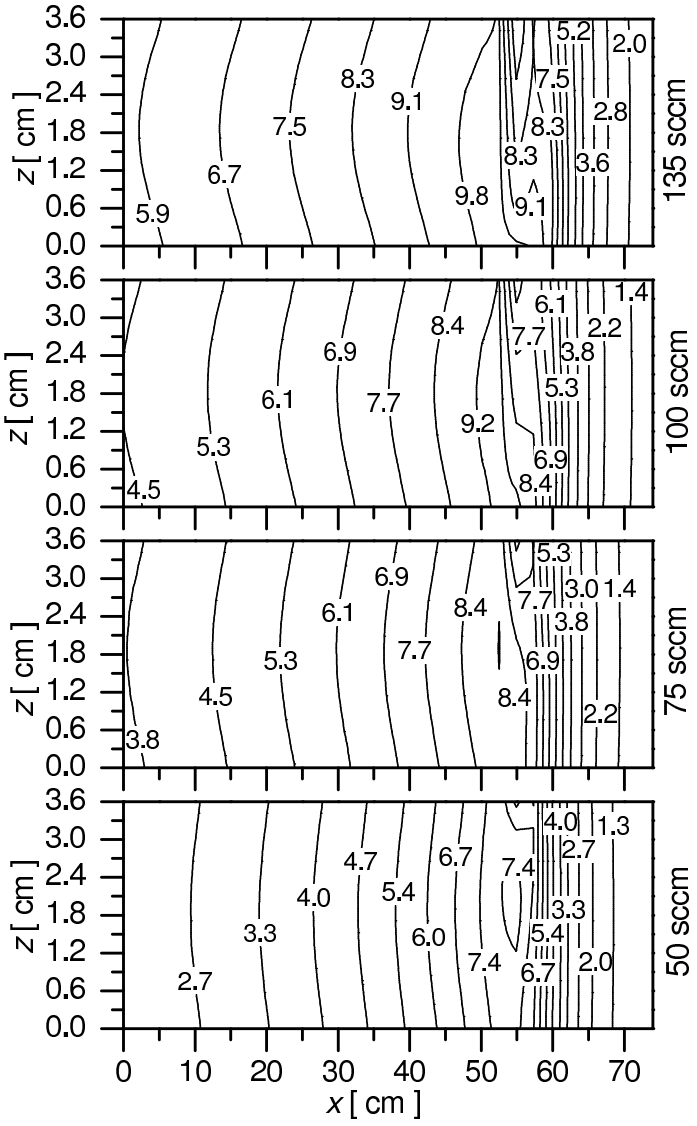

Figure 13. Calculated O_2(a) density distributions in the vertical symmetry plane of the reactor at different gas flow rates, when the pressure in the reactor is kept constant at 50 Pa. The densities are given in 10^{20} m^{-3} units.

at this flow rate the pressure in the discharge region is in the range (140 Pa) where the dissociation rate does not change considerably with small Ar [52] addition, such as 10%, and therefore the absolute O-atoms density can decrease more pronouncedly. Nevertheless in most part of the reactor similar densities can be achieved as in the 100% O_2 case, as also showed by the density distributions presented in Figure 15. Concerning the O_2(a) molecules, comparing to the 100% O_2 case slightly lower densities are achieved along the reactor. As shown in Figure 16 at high flows the density decreases moderately along the reactor from the inlet towards the outlet, while at the lowest investigated gas flow rate the density decreases approximately a factor of 3. The O_2(a) density profiles in the reactor are similar to those of O-atoms shown in Figure 15. A separate control of

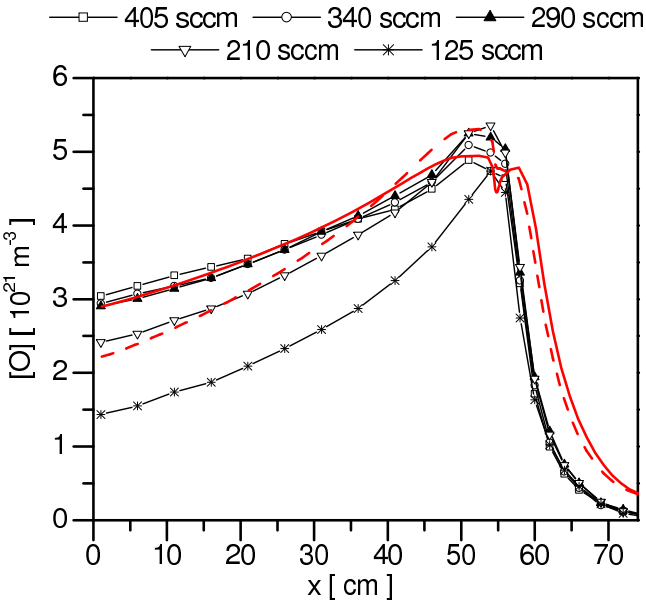

Figure 14. Axial distribution of measured oxygen atom densities along the middle axis of the reactor at different gas flow rates, when the pressure in the reactor is kept constant at 100 Pa in the case of 90%O_2-10%Ar mixture. The lines in the figure represent the calculated densities at 405 sccm (——) and 210 sccm (– – –) gas flow rates.

these species at a given pressure, as their density being determined mostly by surface processes, can be achieved by changing the surface recombination probability of species. In case of O-atoms this can be easily achieved by the heating of the surface. On the other hand, as seen in the previous section, the O_2(a) densities can be manipulated by changing the pressure, i.e. the reduction of pressure results in the decrease of the relative density of excited molecules.

5. Conclusions

In the present work we have studied the tuning possibility of species density distributions in the afterglow of a surface-wave microwave discharge with a special configuration, where the discharge tube was positioned perpendicularly to the afterglow tube at about 2/3 of its length. The afterglow tube was pumped through its farther end from the discharge tube connection and closed at the other end. The characteristics of this special geometry afterglow system have been determined by modelling calculations, and the effect of the gas flow rate on the density distributions in the reactor has been extensively studied. The validity of the models has been shown by the comparison of the calculated and measured axial distribution of O-atoms.

The calculations revealed important features of the system, such as: (*i*) due to the perpendicular injection of the plasma jet into reactor the gas temperature is close to the room temperature in most part of the reactor except a 5 cm region around the inlet; (*ii*)

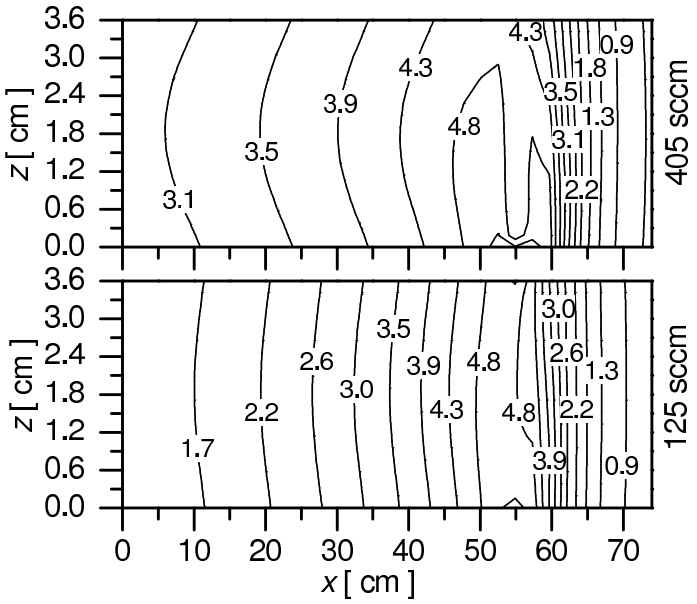

Figure 15. Calculated O-atoms density distributions in the vertical symmetry plane of the reactor at two different gas flow rates, when the pressure in the reactor is kept constant at 100 Pa in 90%O_2-10%Ar mixture. The densities are given in 10^{21} m^{-3} units.

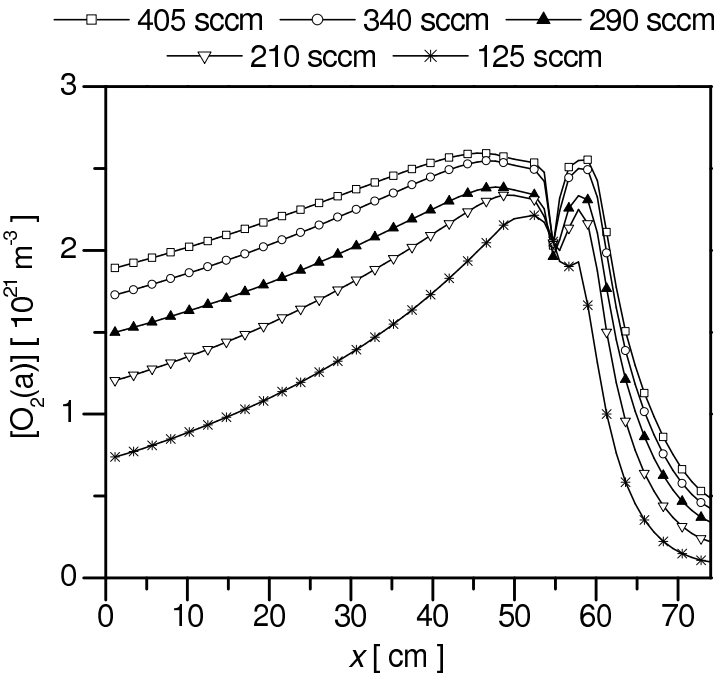

Figure 16. Axial distribution of calculated O_2(a) densities along the middle axis of the reactor at different gas flow rates, when the pressure in the reactor is kept constant at 100 Pa in the case of 90%O_2-10%Ar mixture.

the pressure drop along the discharge tube, which results the change of pressure in the discharge region with the gas flow rate induces the variation of the relative density of

active species entering the reactor, where the pressure is kept constant; (*iii*) the surface recombination probability of atoms varies along the afterglow tube due to the surface temperature gradient, as well as due to the conditioning of the surface resulting from the continuous operation of the system; (*iv*) due to the special structure of the system the density distribution is separately controlled in the two regions of the afterglow tube defined by the position of entrance and pumping positions. The system geometry has been shown to be very practical in applications where surfaces/porous materials are to be treated homogeneously by pumping active species through them, since by tuning the gas flow rate equidensity surfaces can be obtained.

Concerning the active species, it has been shown that the most abundant species in the afterglow of the O_2 surface-wave microwave discharge, with possible role in different applications are the O-atoms and O_2(a) molecules. Their density distributions in the reactor are predominantly determined by the gas flow rate and the quality of the reactor surface (defining the recombination probability of species on the surface). Due to the large gas temperature gradient around the entrance the maximum species densities are obtained not in the plasma jet, but shifted towards the lower temperature zones in the pumping direction. This effect disappears with decreasing the gas flow rate. At 100 Pa at the highest gas flow rate the O-atoms density decreases about a factor of 2 towards the exit, while at the lowest gas flow rate with a factor of 4. At 50 Pa pressure, where also lower gas flow rates have been used, at the highest gas flow rate the same decrease can be obtained as at 100 Pa, however at the lowest gas flow rate the density decrease is about a factor of 6. In the case of O_2(a) molecules at 100 Pa more homogeneous distributions are obtained, i.e. at the highest gas flow rate the density decreases with a factor of 1.5 from the entrance to the exit, while at the lowest gas flow rate the difference is a factor of 2.5. Similar behaviour has been found also at 50 Pa pressure, however contrary to the O-atoms the density of molecules at this pressure is considerably lower than at 100 Pa. On the other hand, in the direction of the closed end of the reactor, that is a diffusion dominated region, the densities decrease at a very high rate. With the addition of Ar to O_2 no significant changes has been observed in the behaviour of the species densities evolution along the reactor.

Acknowledgments

The work has been supported by Hungarian Science Foundation OTKA through K-104531 and Hungarian-Slovenian Intergovernmental bilateral project TÉT-10-1-2011-0638. The authors gratefully acknowledge Vasco Guerra and Paulo A Sá for their contribution to the development of the discharge model.

References

[1] Mozetic M, Cvelbar U, Sunkara M K and Vaddiraju S 2005 *Adv. Mater.* **17** 2138–42
[2] Cvelbar U 2011 *J. Phys. D: Appl. Phys.* **44** 174014

[3] Belmonte T, Gries T, Cardoso R P, Arnoult G, Kosior F and Henrion G 2011 *Plasma Sources Sci. Technol.* **20** 024004–7
[4] Wang H, Tang H Z, He J H and Wang Q W 2009 *Mater. Res. Bull.* **44** 1676–80
[5] Lim S T, Kim G H and Jeong G H 2012 *J. Korean Physical Society* **61** 1083–87
[6] Cui S, Mattson E C, Lu G, Hirschmugl C, Gajdardziska-Josifovska M and Chen J 2012 *J. Nanopart. Res.* **14** 744
[7] Vesel A 2010 *Surf. Coatings Techn.* **205** 490–7
[8] Cvelbar U *et al* 2007 *Appl. Surf. Sci.* **253** 8669–73
[9] Jokinen V, Suvanto P and Franssila S 2012 *Biomicrofluidics* **6** 016501
[10] Wang X W, Hu J and Liang Y 2012 *E-J. Chem.* **9** 1581–6
[11] Masaeli E, Morshed M and Tavanai H 2007 *Surf. Interface Anal.* **39** 770–4
[12] Lei M K, Liu Y and Li Y P 2011 *Appl. Surf. Sci.* **257** 7350–8
[13] Modic M, Junkar I, Vesel A and Mozetic M 2012 *Surf. Coat. Technol.* **213** 98–104
[14] Cvelbar U, Modic M, Kovac J, Filipic G, Junkar I, Elersic K and Mozetic M 2012 *Surf. Coat. Technol.* **211** 200–4
[15] Zanden C, Voinova M, Gold J, Morsdorf D, Bernhardt I and Liu J H 2012 *Eur. Polym. J.* **48** 472–82
[16] Liu X M, Wu S L, Yeung, K W K, Chung C Y and Chu P K 2012 *Int. J. Electrochem. Sci.* **7** 6638–53
[17] Cvelbar U, Mozetic M, Hauptman N and Klanjsek Gunde M 2009 *J. Appl. Phys.* **106** 103303
[18] Lee K, Paek K H, Ju W T and Lee Y 2006 *J. Microbiol.* **44** 269–75
[19] Nagatsu M, Terashita F, Nonaka H, Xu L, Nagata T and Koide Y 2005 *Appl. Phys. Lett.* **86** 211502
[20] Lim J P, Uhm H S and Li S Z 2007 *Phys. Plasmas* **14** 093504
[21] Bol'shakov A A, Cruden B A, Mogul R, Rao M V V S, Sharma S P, Khare B N and Meyyappan M 2004 *AIAA J.* **42** 823–32
[22] Lazovic S *et al* 2010 *New J. Phys.* **12** 083037
[23] Uhm H S, Choi E H, Cho G S and Hong Y C 2012 *J. Korean Physical Society* **60** 897–902
[24] Uhm H S and Hong Y C 2011 *Thin Solid Films* **519** 6974–80
[25] Yang L Q, Chen J R, Gao J L and Guo Y F 2009 *Appl. Surf. Sci.* **255** 8960–4
[26] Moisan M and Zakrzewski Z 1991 *J. Phys. D: Appl. Phys.* **24** 1025
[27] Boudam M K, Saoudi B, Moisan M, Ricard A 2007 *J. Phys. D: Appl. Phys.* **40** 1694
[28] Kutasi K , Saoudi B, Pintassilgo C D, Loureiro J, Moisan M 2008 *Plasma Process. Polym.* **5** 840
[29] Kutasi K, Guerra V and Sá P 2011 *Plasma Sources Sci. Technol.* **20** 035006
[30] Kutasi K and Loureiro J 2007 *J. Phys. D: Appl. Phys.* **40** 5612
[31] Hacker D S, Marshall S A and Steinberg M 1961 *J. Chem. Phys.* **35** 1788
[32] Cvelbar U, Mozetic M and Ricard A 2005 *IEEE Trans. Plasma Sci.* **33** 834–7
[33] Babic D, Poberaj I and Mozetic M 2001 *Rev. Sci. Instrum.* **72** 4110–4
[34] Zaplotnik R, Vesel A and Mozetic M 2012 *Sensors* **12** 3857–67
[35] Booth J, Joubert O, Pelletier J and Sadeghi N 1991 *J. Appl. Phys.* **69** 618–26
[36] Macko P, Veis P and Cernogora G 2004 *Plasma Sources Sci. Technol.* **13** 251–62
[37] Dimauro L, Gottscho R and Miller T 1984 *J. Appl. Phys.* **56** 2007–11
[38] Corr C S, Gomez S and Graham W G 2012 *Plasma Sources Sci. Technol.* **21** 055024
[39] Dal'Maz Silva W, Belmonte T, Duday D, Frache G, Noel C, Choquet P, Migeon H-N, Maliska A 2012 *Plasma Process. Polym.* **9** 207
[40] Noel C, Kutasi K, Belmonte T "Oxidizing species in late Ar-O2-N2 afterglow for bacterial treatment" 2012 Book of abstracts of 4th international conference on plasma medicine, June 17-21, Orlans - France, 2012, Ed: M. Mikikian, H. Rabat, E. Robert, J-M. Pouvesle, p.183; Defais T, Noel, Belmonte T, Henrion G 2012 in Proc. ESCAMPIG XXI, Viana do Castelo, Portugal, contribution 109
[41] Ferreira C M 1983 *J. Phys. D: Appl. Phys.* **16** 1673

[42] Ferreira C M and Loureiro J 1984 *J. Phys. D: Appl. Phys.* **17** 1175
[43] Guerra V and Loureiro J 1999 *Plasma Sources Sci. Technol.* **8** 110
[44] Pintassilgo C D, Loureiro J, Guerra V 2005 *J. Phys. D: Appl. Phys.* **38** 417
[45] Guerra V, Sá P A and Loureiro J 2001 *Phys. Rev. E* **63** 046404–1–13
[46] Kutasi K, Pintassilgo C D, Coelho P J, Loureiro J 2006 *J. Phys. D: Appl. Phys.* **39** 3978
[47] Kutasi K, Guerra V and Sá P 2010 *J. Phys. D: Appl. Phys.* **43** 175201
[48] Pinheiro M J, Gousset G, Granier A, Ferreira C M 1998 *Plasma Sources Sci. Technol.* **7** 524
[49] Gordiets B, Ferreira C M, Guerra V, Loureiro J, Nahorny J, Pagnon D, Touzeau M, Vialle M 1995 *IEEE TRans. Plasma Sci.* **23** 750
[50] Clement F, Lecoq E, Duday D, Belmonte T, Audinot J-N, Lentzen E, Penny C, Cauchie H-M and Choquet P 2011 *New Journal of Physics* **13** 113040
[51] Guerra V, Kutasi K and Sá P 2010 *Appl. Phys. Lett.* **96** 071503
[52] Kutasi K, Sá P and Guerra V 2012 *J. Phys. D: Appl. Phys.* **45** 195205